Slip tendency analysis as a tool to constrain fault reactivation: A numerical approach applied to three-dimensional fault models in the Roer Valley rift system (southeast Netherlands)

Geza Worum,[1] Jan-Diederik van Wees,[2] Gabor Bada,[1] Ronald T. van Balen,[3] Sierd Cloetingh,[1] and Henk Pagnier[2]

Received 14 May 2003; revised 29 August 2003; accepted 6 November 2003; published 4 February 2004.

[1] We describe a new numerical approach to constrain the three-dimensional (3-D) pattern of fault reactivation. Taking advantage of the knowledge of the tectonic stress field, the ratio of the resolved shear and normal stresses (slip tendency) as well as the direction of the shear stress is calculated at every location on the faults modelled by triangulated surfaces. Although the calculated contact stresses represent only a first order approximation of the real stresses, comparison of the 3-D pattern of slip tendency with the frictional resistance of the fault can provide useful constraints on the probability of fault reactivation. The method was applied to 3-D geometrical fault models in the Roer Valley Rift System (southeast Netherlands) which is presently characterized by pronounced tectonic activity. The input stress tensors were constrained by published stress indicators. The analysis demonstrated that the observed fault activity could be explained within a reasonable range of frictional parameters and input stress magnitudes. In addition a fairly good correlation was found between the predicted slip directions and the focal mechanisms of local earthquakes. This suggests that in the study area, fault models being valid in the uppermost part of the crust are suitable to constrain fault reactivation even in the deeper part of the seismogenic layer. The analysis further demonstrated that fault hierarchy and the regional tectonic contexts of the fault system are important factors in fault reactivation. Therefore they always should be taken into account during evaluation of the calculated slip tendency and slip direction patterns. *INDEX TERMS:* 3210 Mathematical Geophysics: Modeling; 8010 Structural Geology: Fractures and faults; 8107 Tectonophysics: Continental neotectonics; 8164 Tectonophysics: Stresses—crust and lithosphere; 9335 Information Related to Geographic Region: Europe; *KEYWORDS:* three-dimensional modeling, fault reactivation, northwest Europe

Citation: Worum, G., J.-D. van Wees, G. Bada, R. T. van Balen, S. Cloetingh, and H. Pagnier (2004), Slip tendency analysis as a tool to constrain fault reactivation: A numerical approach applied to three-dimensional fault models in the Roer Valley rift system (southeast Netherlands), *J. Geophys. Res.*, *109*, B02401, doi:10.1029/2003JB002586.

1. Introduction

[2] Understanding and prediction of the behavior of preexisting faults in a certain tectonic stress field is important in many fields of geosciences. For example, adequate estimation of the resolved stresses along known or suspected faults is very important in exploring high-risk and earthquake-prone blind faults and ultimately in assessing seismic hazard. In the oil industry the effect of oblique faulting on the geometry of reservoirs is an important issue. However, using classical exploration methods (seismic surveys) only the normal component of the displacement field can be easily observed, usually the sense and relative magnitude of the lateral component remain undetected. Furthermore fault sealing, which is of crucial importance in hydrocarbon migration and reservoir geology depends also on the displacement and the actual stresses of the faults [e.g., *Grauls and Baleix*, 1994; *Sibson*, 1994].

[3] Accurate prediction of fault reactivation can only be given using sophisticated methods such as the 3-D finite element modeling approach. However, if the model contains many faults, these methods have the disadvantage of being complex and very time consuming in terms of both preparation and computation. Coarsening the mesh in these situations speeds up the calculation, but it often results in a solution significantly deviating from reality.

[4] Several frequently used forward methods have been developed, which aim to quickly model the fault behavior in a certain tectonic stress field. These methods estimate the probability and/or sense of reactivation using either a graphical approach (Mohr circles) [e.g., *Jaeger and Cook*, 1976; *Ranalli*, 1987; *Twiss and Moores*, 1992] or an

[1]Department of Tectonics, Vrije Universiteit, Amsterdam, Netherlands.
[2]Department of Geoenergy, Nederlands Instituut voor Toegepaste Geowetenschappen TNO, Utrecht, Netherlands.
[3]Department of Quaternary Geology and Geomorphology, Vrije Universiteit, Amsterdam, Netherlands.

0148-0227/04/2003JB002586$09.00

analytical approach [*Sibson*, 1985; *Yin and Ranalli*, 1992; *Morris et al.*, 1996; *Pascal*, 1998; *Alaniz-Alvarez et al.*, 2000; *Pascal et al.*, 2002]. The advantage of these forward techniques is that they are simple, quick and (some of them) can handle large number of faults simultaneously. All of these techniques use the Wallace-Bott hypothesis [*Wallace*, 1951; *Bott*, 1959] which follows 5 main assumptions: (1) faults are planar and infinite; (2) displacement along the faults is small; (3) fault blocks are rigid and no block rotation occurs; (4) displacement is independent from displacement on other faults (no fault interactions) and (5) a single homogeneous stress field is considered responsible for the displacements. It is important to note that these forward approaches are the opposite of the more popular and widely used stress inversion methods, which use the same Wallace-Bott assumption [e.g., *Angelier*, 1984; *Gephart and Forsyth*, 1984; *Reches*, 1987; *Gephart*, 1990; *Yin and Ranalli*, 1995; *Yamaji*, 2000]. The disadvantages of these either forward or backward techniques is that the calculated contact forces are based on significant simplifications of reality, neglecting many important factors such as fault interaction, fault block rotation and fault block deformation. Numerous fault reactivation studies were performed in the past using the Wallace-Bott hypothesis. None of these however, suggested that the deviation between the theoretical and actual resolved stresses along the faults would be statistically significant, since the predicted fault behavior was found to be consistent with the Wallace-Bott approach [e.g., *Zoback and Zoback*, 1980; *Zoback et al.*, 1981; *Gephart and Forsyth*, 1984; *Bergerat*, 1987; *Rebaï et al.*, 1992]. Numerical studies performed by *Dupin et al.* [1993] and *Pollard et al.* [1993] have quantitatively evaluated the error of the Wallace-Bott approach in various geological situations. They found that the deviation between the actual slip direction and the slip direction predicted by the ''far-field'' approach is lower than 30° and as an average is below 10°. Thus the above mentioned field and numerical studies have empirically and quantitatively demonstrated the applicability of the Wallace-Bott hypothesis as a first order approximation.

[5] In agreement with the Wallace-Bott hypothesis the earlier mentioned forward techniques always used 2D or planar fault geometries to estimate fault behavior in a certain stress field, even if the detailed 3-D geometry of the fault system was available (typically in the case of subsurface exploration by the petroleum industry). By doing so some important aspects of fault reactivation related to changing fault shape/orientation could remain undetected.

[6] In this paper we present a new analytical technique which utilises the full 3-D fault geometry revealed by geological data in order to estimate the 3-D pattern of forces acting along the pre-defined faults. This approach also uses the Wallace-Bott hypothesis, the resulting 3-D pattern of resolved stresses therefore represents only a first order approximation of the real forces arising along the given fault surfaces. We use the calculated force pattern to provide useful constraints on fault reactivation. Faults or fault regions, where the calculated shear forces overcome the frictional resistance of the fault are considered to be the likely location of fault reactivation.

[7] In this paper first the modeling approach is presented in detail including the modeling steps, inputs, mathematical principles, outputs and their relationship with fault reactivation. Then the modeling procedure is demonstrated on a synthetic example followed by a detailed discussion about the accuracy and reliability of the modeling. Finally the technique presented here is applied to 3-D fault models in the SE Netherlands, which is presently characterized by pronounced tectonic activity.

2. Modeling Approach

2.1. Modeling Concept

[8] We aim at simulating the 3-D pattern of contact forces arising along faults in a certain tectonic stress field in order to provide constraints on the 3-D pattern of fault reactivation. The calculation of the resolved stresses is based on the Wallace-Bott hypothesis: at every location on the 3-D fault surface the resolved shear and normal stresses are calculated using the local normal vector of the fault at the given location and the regional tectonic stress field. In a dynamic way local distortion of the stress field due to fault interaction, fault shape and fault block rotations are not taken into account. As mentioned in the introduction our approach is inverse to the more widely used stress inversion methods, which use kinematic data collected in the field or focal mechanism solutions of earthquakes to reconstruct the paleo- or recent stress field [e.g., *Angelier*, 1984, 1990, 2002; *Reches*, 1987; *Gephart and Forsyth*, 1984; *Gephart*, 1990; *Yin and Ranalli*, 1995; *Yamaji*, 2000]. The technique presented here works the opposite way: it takes advantage of the knowledge of the regional stress field in order to estimate the stress pattern along pre-existing faults. The calculated force pattern is used to provide useful constraints on fault reactivation. Faults or fault regions, where the calculated shear forces overcome the frictional resistance of the fault are considered to be a probable location of fault reactivation.

2.2. Modeling Procedure

[9] The presented numerical analysis follows three major steps. During the first step, the 3-D geometrical model of the fault pattern is prepared and the confining stress field is determined. It is to be emphasised that the method yields reliable results only if both the 3-D fault geometry and the recent stress field in the study area are well constrained. The fault models are generally created from fault trace lines corresponding to various geological horizons, from geological cross sections, from 2 or 3 dimensional seismic surveys and/or from direct field observations. The 3-D fault models are represented by triangulated surfaces and are created using the commercial software package GOCAD.

[10] During the second step the magnitudes of contact stresses as well as the direction of the resolved shear stress are calculated at every location of the 3-D fault models (details later), for this purpose a Java2 computer tool was developed. The inputs for the software are the 3-D fault models as well as the parameters describing the stress field. Another parameter is calculated, namely the ratio of the resolved shear and normal stress magnitudes (slip tendency after *Morris et al.* [1996]), which is an important parameter in fault reactivation studies.

[11] During the third step in the numerical analysis, the statistical and/or visual evaluation of the computed param-

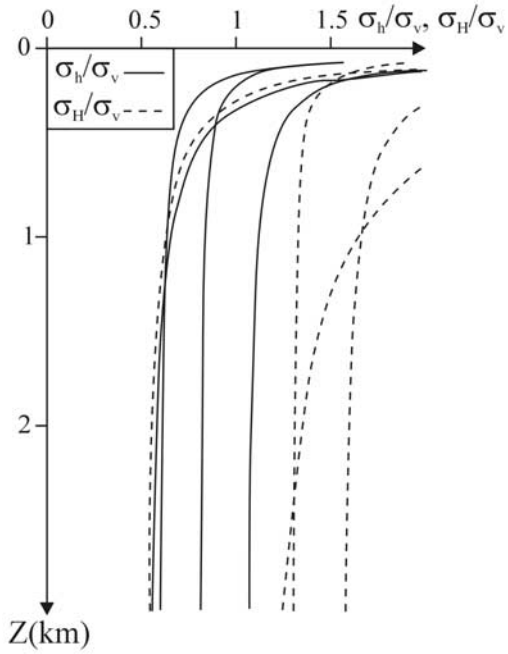

Figure 1. Depth dependency of measured horizontal principal stresses (σ_h and σ_H) normalized with respect to the vertical principal stress (σ_v) for hydrofrac tests in different boreholes with depth $z > 500$ m. (for data and references see *Rummel* [1986]). Below a certain depth (transition depth: ~1 km) the principal stress ratios can be considered to be constants.

eters is carried out. For this purpose the commercial software GOCAD is used, which is also suitable for any further processing of the output parameters (e.g., corrections). Analysis of the resolved stresses in order to constrain the reactivation pattern of the faults is performed during this step.

2.2.1. Input Stress Field Assumptions

[12] Regarding the input stress field we assume that it is everywhere (1) Andersonian (one of the principal stresses is vertical) and (2) follows a simple, linear trend with depth in agreement with various observations [*Jaeger and Cook*, 1976; *Brudy et al.*, 1997; *Plenefisch and Bonjer*, 1997]. Lateral variation of the magnitude/orientation of the input stress field is allowed, but at every location a simple linear depth-dependency is assumed. Parameters describing these conditions serve as inputs for the software. Following *Rummel* [1986], the observed depth-dependency of the principal stresses can be summarized as (Figure 1):

$$R_h(z) = \frac{\sigma_h(z)}{\sigma_v(z)} = \frac{\gamma_h}{z} + \beta_h$$
$$R_h(z) = \frac{\sigma_H(z)}{\sigma_v(z)} = \frac{\gamma_H}{z} + \beta_H \quad (1)$$

where γ_h, γ_H, β_h, β_H are constants. σ_H, σ_h and σ_v represent the maximum horizontal, the minimum horizontal and the vertical principal stresses respectively. Figure 1 reveals, that below a certain depth (~0.3–1 km depending on the asymptotic stress ratio and the γ value) the σ_h/σ_v and σ_H/σ_v ratios can be considered as being depth-independent values. This means that the linear depth dependence of the principal stresses having the following form adequately describes the stress field at greater depth [e.g., *Jaeger and Cook*, 1976; *Ito and Zoback*, 2000]:

$$\sigma = K \cdot z \quad (2)$$

where σ is one of the principal stresses in general and K is constant.

[13] This form of depth dependency of the principal stresses is ideal for the fault reactivation analysis. Namely, since neither the slip tendency nor the slip direction depends on the absolute magnitude of the stress tensor (described in detail later), we can represent the stress model described by equation (2) at every location by a uniform stress tensor. It has three independent parameters: the orientation of σ_H and the σ_h/σ_H and σ_v/σ_H ratios respectively. The form of this reduced stress tensor is:

$$\underline{\underline{\sigma}} = \begin{pmatrix} 1 & 0 & 0 \\ 0 & \sigma_h/\sigma_H & 0 \\ 0 & 0 & \sigma_v/\sigma_H \end{pmatrix} \quad (3)$$

Summing up, the depth dependency of the input stress fields in our approach is assumed to be linear and can be described either by equation (1) or by equation (2). Regarding the fault reactivation, the tensor form of equation (3) is equivalent with equation (2).

2.2.2. Mathematical Principles and Outputs

[14] Let us assume a stress field where one of the three static principal stresses is vertical (Andersonian). This stress tensor in its eigensystem has the following, diagonal form:

$$\underline{\underline{\sigma}}_E = \begin{pmatrix} \sigma_H & 0 & 0 \\ 0 & \sigma_h & 0 \\ 0 & 0 & \sigma_v \end{pmatrix} = \sigma_H \cdot \begin{pmatrix} 1 & 0 & 0 \\ 0 & \sigma_h/\sigma_H & 0 \\ 0 & 0 & \sigma_v/\sigma_H \end{pmatrix} \quad (4)$$

where σ_H, σ_h and σ_v represent respectively the maximum horizontal, the minimum horizontal and the vertical principal stresses. This stress field in the reference geological co-ordinate system (O, East, North, Up) has the tensor form of:

$$\underline{\underline{\sigma}} = \underline{\underline{\Omega}} \cdot \underline{\underline{\sigma}}_E \cdot \underline{\underline{\Omega}}^T \quad (5)$$

where $\underline{\underline{\Omega}}$ is the matrix describing the transformation between the geological co-ordinate system and the eigensystem of $\underline{\underline{\sigma}}_E \cdot \underline{\underline{\Omega}}$ is a rotational matrix and can be written as:

$$\underline{\underline{\Omega}} = \begin{pmatrix} \cos(\theta) & \sin(\theta) & 0 \\ \sin(\theta) & -\cos(\theta) & 0 \\ 0 & 0 & 1 \end{pmatrix} \quad (6)$$

where θ is the azimuth of σ_H. The θ is measured clockwise from north (y axis).

[15] The normal unit vector at every location on the surface is denoted by $\underline{n}$(x, y, z). The $\underline{F}$ force, which acts along the surface as it is subjected to the $\underline{\underline{\sigma}}$ stress field as

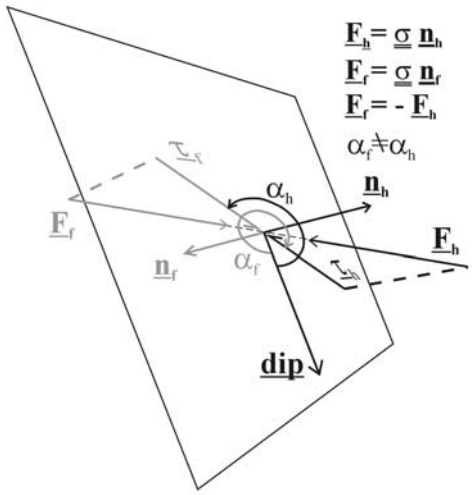

Figure 2. Forces (($\underline{F}_f$) and ($\underline{F}_h$)) and their shear components ($\underline{\tau}_f$ and $\underline{\tau}_h$) acting between the two sides of a fault surface element in a stress field represented by the stress tensor σ. The shear direction ($\underline{\alpha}$) is defined by the angle between the dipline and the shear vector (equation (12)). See text for further discussion.

well as its normal and shear components respectively are given by the following vector operations:

$$\underline{F} = \underline{\underline{\sigma}} \cdot \underline{n} \tag{7}$$

$$\underline{\sigma}_n = (\underline{F} \cdot \underline{n}) \cdot \underline{n} = \left(\underline{n} \cdot \underline{\underline{\sigma}} \cdot \underline{n}\right) \cdot \underline{n} \tag{8}$$

$$\underline{\tau} = \underline{F} - \underline{\sigma}_n \tag{9}$$

where $\underline{\sigma}_n$ and $\underline{\tau}$ denote the normal and shear component of the $\underline{F}$ force respectively. The slip tendency [after *Morris et al.*, 1996], which is an important parameter in the reactivation analysis is defined by the ratio of the shear and normal stress magnitudes:

$$ST(x,y,z) = \frac{\|\underline{\tau}\|}{\|\underline{\sigma}_n\|} \tag{10}$$

In the eigensystem of the stress tensor (x′, y′, z′ co-ordinate system) where $\underline{\underline{\sigma}} = \underline{\underline{\sigma}}_E$, by combining (4), (8), (9) and (10) the slip tendency yields the following form:

$$ST(x',y',z') = \frac{\sqrt{n_x^2 + \left(\frac{\sigma_h}{\sigma_H}\right)^2 \cdot n_y^2 + \left(\frac{\sigma_v}{\sigma_H}\right)^2 \cdot n_z^2 - \left(n_x^2 + \left(\frac{\sigma_h}{\sigma_H}\right) \cdot n_y^2 + \left(\frac{\sigma_v}{\sigma_H}\right) \cdot n_z^2\right)^2}}{n_x^2 + \left(\frac{\sigma_h}{\sigma_H}\right) \cdot n_y^2 + \left(\frac{\sigma_v}{\sigma_H}\right) \cdot n_z^2} \tag{11}$$

where n_x, n_y and n_z denote the x, y and z components respectively of the normal vector of the surface element described in the eigensystem of the stress tensor. It is important to note that the slip tendency does not depend on the absolute magnitude of the principal stresses. It depends only on the ratios of the principal stresses and on the relative orientation of the fault.

[16] As it was discussed by *Wallace* [1951] and more recently by *Pascal and Angelier* [2004], the direction of the shear vector also depends only on the relative magnitude of the principal stresses and the orientation of the fault. Since the direction of the shear vector is generally associated with the direction of slip [*Wallace*, 1951; *Bott*, 1959; *Pascal et al.*, 2002] the absolute magnitude of the stress tensor is irrelevant regarding the fault reactivation. The normalised form of the stress tensor (equation (3)) therefore is an adequate input for the calculation.

[17] For evaluation and visualisation purposes, the shear direction was calculated also as a scalar value. This is represented by the α angle measured counter-clockwise between the direction of local dip and the direction of the shear vector (see Figure 2). The crossproduct of the unit dipline vector and the normalised shear vector enables us to determine the αslip direction in the full 0°–360° range:

$$\alpha = \sin^{-1}\left(\left\|\underline{dip} \times \frac{\underline{\tau}}{\|\underline{\tau}\|}\right\|\right) \qquad \text{if} \quad \left(\underline{dip} \times \frac{\underline{\tau}}{\|\underline{\tau}\|}\right) \cdot \underline{n} > 0 \tag{12a}$$

$$\alpha = 180 + \sin^{-1}\left(\left\|\underline{dip} \times \frac{\underline{\tau}}{\|\underline{\tau}\|}\right\|\right) \quad \text{if} \quad \left(\underline{dip} \times \frac{\underline{\tau}}{\|\underline{\tau}\|}\right) \cdot \underline{n} < 0 \tag{12b}$$

α values of 0° and 360° represent normal, while 180°, 90° and 270° represents respectively pure reverse, left and right lateral movements.

[18] From a mathematical point of view, the definition of the slip direction raises a problem, which is related to the chosen normal vector (Figure 2). The same fault can be oriented either by a normal vector pointing toward the interior of the hangingwall block ($\underline{n}_h$) or by $\underline{n}_f$, which is the normal vector oriented oppositely. In case of shear faulting $\underline{F}_h$($\underline{F}_f$) represents the pushing force of the hangingwall (footwall) block acting on the footwall (hangingwall) block. The relative movements of the two blocks along the fault, which are represented by the shear components of $\underline{F}_h$ and $\underline{F}_f$ are parallel but have opposite direction. However, since α is defined as in equation (12), α_h does not equal α_f. This can lead to confusion if one wants to compare slip direction on faults oriented by the opposite normal vector. To avoid this confusion, both α_h representing the slip direction of the hangingwall block relative to the footwall block and α_f representing the slip direction of the footwall block relative to the hangingwall block are calculated.

[19] The above formulas were implemented into the developed Java2 application to calculate the pattern of resolved stresses at every location along the 3-D fault. As outputs, the software provides the fault surfaces with calculated shear stress vectors, slip tendencies and slip directions (α_h and α_f) as properties stored by the fault nodes.

2.2.3. Slip Tendency and Fault Reactivation

[20] We use the calculated pattern of resolved stresses to constrain the spatial pattern of fault reactivation. It is

assumed that slip occurs in the direction of the resolved shear stress (Wallace-Bott hypothesis) if it is larger than the frictional resistance of the fault [*Jaeger and Cook*, 1976]:

$$\tau \geq S_0 + \mu_{slide} \cdot (\sigma_n - P_{Hidr})$$
$$ST \geq \frac{S_0}{\sigma_n} + \mu_{slide} \cdot \left(1 - \frac{P_{Hidr}}{\sigma_n}\right) \quad (13)$$

where ST is the slip tendency, τ and σ_n are respectively the shear and normal stress magnitudes along the fault under normal pore pressure conditions, S_0 and μ_{slide} are respectively the cohesion and coefficient of frictional sliding of the fault, and P_{Hidr} is the overpressure of the pore fluid. As one can see, a correlation exists between slip tendency and fault reactivation: higher slip tendency values imply that the given fault or fault segment is better oriented to the confining stress field, and therefore indicates a higher probability of slip. Whether slip actually occurs is difficult to predict, since it depends on many factors, which are not easy to quantify along the faults. However, considering a reasonable range for the parameters on the right-hand side of equation (13) one can try to use the slip tendency pattern to provide useful constraints on fault reactivation.

[21] Laboratory experiments indicate that cohesion between two sliding surfaces depends on the normal stress [*Byerlee*, 1978] and is found to range between 300–1100 KPa [*Jaeger and Cook*, 1976, p. 60]. As other experiments showed [*Krantz*, 1991], cohesion along fractures generally decreases as subsequent slip occurs (e.g., large faults), but it can also be "healed" by, for example, rock-fluid interactions [*Tenthorey et al.*, 2003]. Several field studies showed however, that neglecting cohesion along pre-existing faults is a realistic assumption [*Brace and Kohlstedt*, 1980; *Reches*, 1987; *Twiss and Moores*, 1992; *Zoback*, 1992; *Plenefisch and Bonjer*, 1997]. This assumption reduces equation (13) to a simpler form:

$$\tau \geq \mu_{slide} \cdot (\sigma_n - P_{Hidr})$$
$$ST \geq \mu_{slide} \cdot \left(1 - \frac{P_{Hidr}}{\sigma_n}\right) = \mu_{eff} \quad (14)$$

where μ_{eff} is the "effective" frictional coefficient. Considering constant shear and normal stress magnitudes slip occurrence is more likely if μ_{eff} is low. This may result either from elevated pore pressure or from a reduced frictional coefficient (μ_{slide}). In reality, slip may result from the combination of both factors: reduced frictional coefficient and slightly elevated pore pressure. In studies evaluating earthquake focal mechanism data [*Zoback*, 1992; *Plenefisch and Bonjer*, 1997], generally the two end-members are considered: (1) pore pressure is assumed to be hydrostatic allowing the frictional coefficient to be determined or (2) frictional coefficient is assumed to be in agreement with laboratory measurements (μ_{slide} = 0.6–1.0 [*Jaeger and Cook*, 1976; *Byerlee*, 1978]) and the elevated pore pressure is determined. Using the first assumption μ_{slide} = 0.3–0.6 range was determined [*Zoback*, 1992; *Plenefisch and Bonjer*, 1997]. Other studies also found frictional coefficients lower (0.2–0.6) than those measured in laboratory [*Reches*, 1987; *Martinez-Diaz*, 2002]. A decreased frictional coefficient along large faults was found to be reasonable and was explained by sliding through a gouge layer and/or the lubricating effect of clay and water [*Brace and Kohlstedt*, 1980; *Hobbs et al.*, 1990].

[22] In this paper the calculated slip tendency values are compared to a reasonable range of frictional coefficients believed to be valid along the faults in order to determine those faults or fault segments, which are likely active in a given stress field. In this idealised case, if the calculated slip tendency overcomes the frictional coefficient of the fault, the probability of slip is predicted to be high. If overpressure, which can be easily quantified using borehole data, is common in the study area, an attempt can be made to calculate the "effective" frictional coefficient as the threshold of possible slip. However, to do that the absolute magnitudes of the resolved normal stresses have to be estimated [e.g., *Zoback*, 1992; *Plenefisch and Bonjer*, 1997].

2.3. Synthetic Example

[23] In order to demonstrate the practical application of the fault reactivation analysis, slip tendency and slip directions were calculated for three faults in a synthetic scenario (Figure 3). For the sake of simplicity a laterally homogeneous, depth dependent stress field described by equation (3) was chosen as input. This stress tensor describes a strike slip regime, with the maximum horizontal principal stress being quasi parallel to fault A. The calculated slip tendency and slip direction values are represented as scalar patterns displayed along the faults in GOCAD. For ease of interpretation, the slip trajectories of the hangingwall blocks are also displayed.

[24] The example demonstrates the impact of changing fault orientation on the reactivation pattern along the faults. The high slip tendency values on the upper part of Fault A (listric fault) and on the left-hand side of fault B indicate that these locations are optimally oriented to the confining stress field. For example if the faults were cohesionless with a frictional coefficient of 0.3 (realistic value), than the upper part of fault A and the left-hand part of fault B would be predicted to more likely slip, than the other part of these faults characterized by lower slip tendency values. The very low calculated slip tendency on fault C indicates that it is not optimally oriented to the stress field, therefore reactivation is unlikely to occur.

[25] The resolved shear directions show how the direction of possible slip varies along the faults as the relative orientation between the fault and the stress field varies. A nice example is fault A, which experiences pure dip slip forces in the left hand side and oblique slip forces at the right hand side.

2.4. Modeling Accuracy

2.4.1. Reliability of the Calculated Resolved Stresses

[26] Several field and numerical examples proved that the "regional stress field" at a given scale is consistent with the kinematics of faults (or fault parts) of the same scale [*Rebaï et al.*, 1992; *Dupin et al.*, 1993; *Hardebeck and Hauksson*, 2001; *Martinez-Diaz*, 2002]. The stress tensor that is called regional, is scale dependent and can be different at different scales. In order therefore to adequately approximate the resolved stresses along mapped faults using the Wallace-

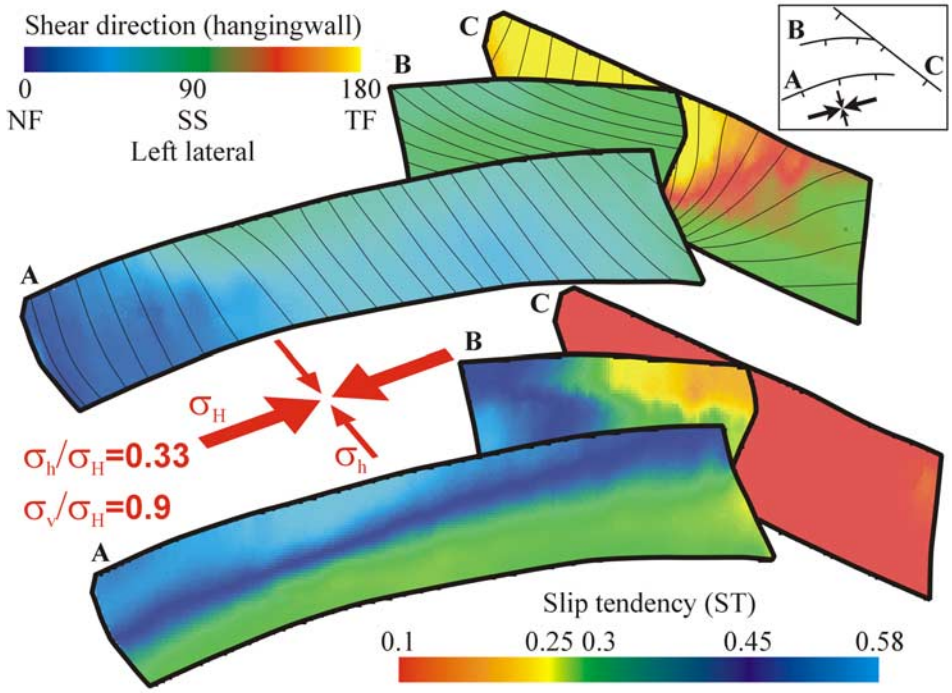

Figure 3. Reactivation analysis of a fictional fault system in a synthetic strike slip stress scenario. Inset shows the map view of the modeled faults. Lower and upper panel show, respectively, the calculated slip tendency and shear directions. Shear trajectories are also shown (thin lines). NF, SS and TF denote normal faulting, strike slip faulting and thrust faulting respectively. See text for further discussion.

Bott hypothesis the confining stress field at the scale of the spatial resolution of the fault models has to be known. If this condition is met, the calculated resolved stresses are reliable. Depending on the number and spatial distribution of the faults this would require stress indicators (borehole breakout, hydrofrac, overcoring etc.) to be available with high spatial density. Since this is seldom the case the input stress field is always "more regional" than would be required, resulting in different degrees of discrepancy between the calculated and the actual resolved stress pattern.

[27] Several numerical and analytical studies were carried out in order to quantify the uncertainty of the Wallace-Bott approach [*Dupin et al.*, 1993; *Pollard et al.*, 1993; *Cashman and Ellis*, 1994; *Nieto-Samaniego and Alaniz-Alvarez*, 1997]. The uncertainty was evaluated in terms of deviation between the calculated and the actual slip directions. The studies show that the effect of the fault length-to-width ratio and the fault depth is negligible (less than 6° deviation). The effect of displacement along a fault on other nearby faults however, can sometimes be significant. For example *Pollard et al.* [1993] found that around a transfer fault connecting two strike-slip faults, the real stress pattern was considerably different from the regional one (~40° deviation in slip direction). Dynamic interaction between two, non-intersecting faults was found to be dependent on the distance between them as well as the style and amount of displacement. If the displacement is small or the distance is large the deviation between the slip directions was concluded as being acceptable (less than 10° deviation). In case of large displacement (due to for example a large earthquake [*Cashman and Ellis*, 1994]) or small distance, the discrepancy was determined to range between 20–30° [*Dupin et al.*, 1993; *Pollard et al.*, 1993]. As it turns out from these studies, the effect of dynamic interaction between two faults forming a transfer zone is smaller if the fault displacement contains less of a strike-slip component. As *Pollard et al.* [1993] pointed out conjugate faults, which are interpreted as forming in one episode of deformation can also interact. "If their spacing is wide relative to their length, interaction is weak, so slip direction is controlled by the regional stress field. However, for closely spaced conjugate faults, interaction may be significant (p. 1050)." Faults can also interact with themselves: Displacement along one part of the fault can distort the regional stress pattern on another part especially around irregularities such as bends and bulges [*Hardebeck and Hauksson*, 2001]. These features which are not uncommon along faults may be located far from the location where the initial displacement occurred.

[28] The significance of these dynamic stress distortions is suggested to depend not only on the fault geometry but also on the deformation rate [*Dupin et al.*, 1993; *Hardebeck and Hauksson*, 2001]. As it was pointed out, if the deformation rate is slow then the tectonic loading driven by far field processes are expected to cancel out these stress variations in the long term. However, in areas characterized by high strain rates and frequent slip periods (e.g., plate boundaries such as southern California [*Hardebeck and Hauksson*, 2001]) there may not be enough time between two subsequent earthquakes to cancel out the stress distortion caused by the previous slip episode. This could result in a very heterogeneous stress field in the long term.

[29] Kinematic interaction between faults occurs in zones where faults are intersecting, since the slip direction is constrained by the geometry of the intersection line. Around

the intersection line the deviation between the resolved stresses calculated using the Wallece-Bott hypothesis and the actual stresses can be significant. This distortion however was estimated to decay rapidly away from the intersection line [*Dupin et al.*, 1993; *Nieto-Samaniego and Alaniz-Alvarez*, 1997].

[30] Besides the mentioned numerical studies, numerous field studies [*Zoback and Zoback*, 1980; *Zoback et al.*, 1981; *Gephart and Forsyth*, 1984; *Bergerat*, 1987; *Rebaï et al.*, 1992; *Zoback*, 1992] also demonstrated that the observed slip data was consistent with the ''far-field approach'' and that the uncertainties were acceptable. These authors have justified, that as a first order approximation the stress pattern calculated using the Wallace-Bott hypothesis is applicable in order to model the actual stresses along faults. Our approach, which is also based on the Wallace-Bott approach does not and can not take dynamically into account phenomena, which deviate the local stress field from the regional one (e.g., fault interaction). In situations when the distortion is expected to be significant (some of them were mentioned earlier) higher uncertainties should be considered in the calculated stress pattern or, if there is available data, the resolution of the input stress field should be increased. Several authors using a similar approach as described in this paper have used the first order approximation of the resolved stresses to estimate fault behavior at different scales [*Morris et al.*, 1996; *Pascal et al.*, 2002; *Ferrill and Morris*, 2003].

2.4.2. Reliability of the Prediction of Fault Reactivation

[31] In this paper the 3-D pattern of calculated resolved stresses are used to constrain the probability and direction of possible fault reactivation. Providing accurate prediction about the 3 dimensional pattern of fault reactivation is not easy. On one hand, the calculation of the resolved stresses are based on simple assumptions, and on the other hand the parameters on the right hand side of equations (13) and (14) describing the reactivation criterion are generally poorly constrained. The frictional coefficient and the cohesion of the faults for example are impossible to measure in situ, and they may vary from fault to fault and even along one particular fault. In addition, several earthquake studies showed that slip on one part of the fault is often the result of displacement on another segment of the same fault [e.g., *Camelbeeck et al.*, 1994; *Pace et al.*, 2002]. The initial slip which is generally located in the deeper part of the seismogenic layer can dynamically generate displacement even at locations where initially the resolved stresses were under the slip threshold. The location of induced slip can be kilometres or even tens of kilometres away from the initial slip [e.g., *Camelbeeck et al.*, 1994]. As it was demonstrated by *Houtgast et al.* [2004] propagation of the induced displacement along an active fault may take considerable time (10^2–10^3 years) in the form of postseismic creep.

[32] Due to the aforementioned difficulties, it would be incorrect to think that the calculated slip tendency values at one location can be directly associated with the likelihood of fault reactivation at the same location. It is more reasonable if the calculated slip tendency pattern is compared to a range of possible slip thresholds (frictional coefficients). With this approach the accuracy (''resolution'') of the reactivation pattern is decreased, but its reliability will be higher. For example if the slip tendency on one fault is lower than the lower limit of a reasonable range of slip thresholds than one could reliably say that the given fault is most likely locked in that particular stress field. Or if the slip tendency is higher than the higher limit of the slip threshold than that fault can be considered reactivation prone.

[33] One should bear in mind that the value of slip tendency correlates with the likelihood rather than the ''amount'' of fault reactivation: higher slip tendency values suggest a higher probability of slip and not more displacement along a given fault. Numerical and field studies showed [e.g., *Dirkzwager et al.*, 2000; *Dirkzwager*, 2002; *Malservisi et al.*, 2003], that the amount of displacement on the surface reflected by the geological record depends primarily on the local rheology, the frictional coefficient and the geometrical parameters of the fault (e.g., length, maximum depth, connectivity). Considering identical orientation and stress field, more displacement is expected for faults which are long and interconnected with the underlying deep crustal fractures than for shallow, secondary faults.

3. Case Study: Slip Tendency Analysis in the SE Netherlands

[34] The study area forms part of the Roer Valley Rift System (RVRS) which is located in the SE part of the Netherlands and adjacent parts of Belgium and Germany (Figure 4). The RVRS is the most tectonically active part of the Cenozoic NW European Rift System [*Ziegler*, 1994], which is one of the major tectonic features of Western Europe.

[35] The RVRS consists of three major tectonic units: The tectonically uplifted Campine and Peel Blocks, which are bounding the central Roer Valley Graben unit from the south and north respectively (Figure 4a). Following the Mesozoic-Early Cenozoic multiphase rifting and inversion periods [*Ziegler*, 1990; *Zijerveld et al.*, 1992; *Geluk et al.*, 1994] the RVRS experienced a renewed rifting which started in the Oligocene and it is still going on today [*Zijerveld et al.*, 1992; *Michon et al.*, 2003]. Recently, the relative tectonic subsidence map inferred from levelling data [*Kooi et al.*, 1998] and the study of the Quaternary deposits and river terraces in the RVRS [*van den Berg*, 1994; *Houtgast and van Balen*, 2000] indicated differential tectonic movements between the Roer Valley Graben and its flanks. This differential subsidence is strongly fault controlled [*Geluk et al.*, 1994; *van den Berg*, 1994; *van den Berg et al.*, 1994; *Houtgast and van Balen*, 2000; *Houtgast et al.*, 2002] and manifested itself in several significant earthquakes in the last century (Figure 4a). Most of these earthquakes are related to slip along the two most important fault zones: the Peel Boundary Fault Zone (PBFZ) and the Feldbiss Fault Zone (FFZ), which separate the central Roer Roer Valley Graben from the Peel and Campine Blocks respectively.

[36] It is generally accepted that far field stresses driven by the Alpine collision control the present-day dynamics of the RVRS [e.g., *Ziegler*, 1990]. In light of this the Cenozoic Roer Valley Graben was interpreted as a transtensional basin [*Kooi et al.*, 1991; *van den Berg*, 1994]. However, Digital Elevation Model [*Michon and van Balen*, 2004] and earthquake focal mechanism studies

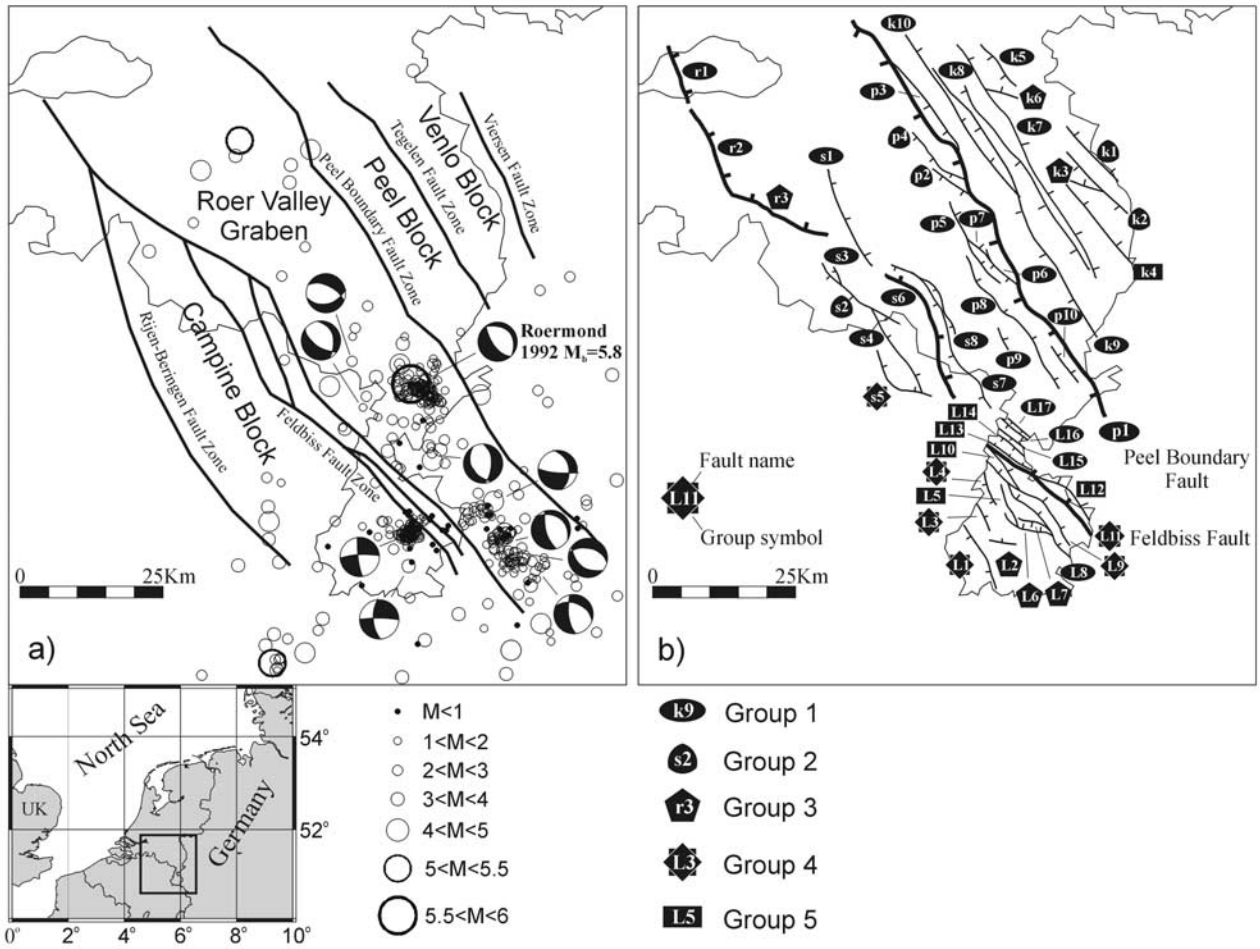

Figure 4. (a) Location and main structural elements of the Roer Valley Rift System. Earthquakes occurred in the last century are shown by circles. Focal mechanisms are after *Camelbeeck and van Eck* [1994]. (b) Map view of the three-dimensional 3-D fault models taking part in the analysis.

[*Camelbeeck et al.*, 1994; *Plenefisch and Bonjer*, 1997] indicated that recently the two border fault zones (PBFZ and FFZ) have experienced displacement with no or minor strike-slip components.

[37] In order to investigate the fault behavior in the RVRS, analysis of the resolved stresses induced by the present-day stress field were carried out. 47 3-D fault models, which were made available by the TNO-NITG Dutch Geological Survey took part in the analysis (Figure 4b). These fault models represent the most important faults in the area but not all of them, since the 3-D fault database is being continuously updated. There is evidence that the faults in the area are not new faults: They have existed since as long as Paleozoic times. This makes the Roer Valley Rift System a suitable area to study the reactivation of pre-existing faults in the present-day tectonic stress field.

3.1. Modeling Assumptions

[38] Regarding the stress field we have to rely upon regional stress indicators, since local data with high spatial density is not available. By inverting the focal mechanism data of the 1992 Roermond earthquake and its aftershocks *Camelbeeck et al.* [1994] and *Camelbeeck and van Eck* [1994] found that the direction of the maximum horizontal (σ_H) principal stress was N139 degrees. The confidence interval of the stress inversion on the other hand suggests that N135–165° directions are also possible. Borehole breakout analysis carried out in the NE Netherlands indicated a N160° ± 5 σ_H orientation [*Rondeel and Everaars*, 1993]. These observations are in agreement with intraplate stress orientations found in Western Europe [e.g., *Ahorner*, 1975; *Klein and Barr*, 1987; *Müller et al.*, 1992; *Plenefisch and Bonjer*, 1997].

[39] The published stress inversion data constrain also the principal stress magnitudes in the area. The R-value range ($R = (\sigma_2 - \sigma_1)/(\sigma_3 - \sigma_1)$) of 0.25–0.45 found by *Camelbeeck et al.* [1994] using the 1992 Roermond earthquake sequence is in agreement with that of *Plenefisch and Bonjer* [1997] (R = 0.4) who used focal mechanism data from a much larger area (Upper Rhine Graben-Roer Valley Rift System). Both of these authors emphasised that the confidence regions of the stress inversion do not make possible an unequivocal distinction between normal faulting and strike-slip faulting stress regimes.

[40] Based on the aforementioned observations, the following assumptions were made regarding the recent stress field in the study area: (1) due to the lack of available stress indicator data with high spatial density the stress field is

Table 1. Principal Stress Ratios of the Stress Tensors Applied as Inputs During the Analysis[a]

R = 0.25			R = 0.45			R = 0.25			R = 0.45		
σ_h/σ_H	σ_v/σ_H	σ_h/σ_v	σ_h/σ_H	σ_v/σ_H	σ_h/σ_v	σ_h/σ_H	σ_v/σ_H	σ_h/σ_v	σ_h/σ_H	σ_v/σ_H	σ_h/σ_v
0.2	**1.267**	**0.158**	**0.2**	**1.655**	**0.121**	**0.2**	**0.800**	**0.250**	**0.2**	**0.640**	**0.313**
0.3	**1.233**	**0.243**	**0.3**	**1.573**	**0.191**	0.3	0.825	0.364	0.3	0.685	0.438
0.4	1.200	0.333	**0.4**	**1.491**	**0.268**	0.4	0.850	0.471	0.4	0.730	0.548
0.5	1.167	0.429	0.5	1.409	0.355	0.5	0.875	0.571	0.5	0.775	0.645
0.6	1.133	0.529	0.6	1.327	0.452	0.6	0.900	0.667	0.6	0.820	0.732
0.7	1.100	0.636	0.7	1.245	0.562	0.7	0.925	0.757	0.7	0.865	0.809
0.8	1.067	0.750	0.8	1.164	0.688	0.8	0.950	0.842	0.8	0.910	0.879
0.9	1.033	0.871	0.9	1.082	0.832	0.9	0.975	0.923	0.9	0.955	0.942

[a]Stress tensors in the left- and right-hand side describe respectively normal faulting and strike-slip faulting regimes. Stress tensors where any of the principal stress ratios are lower than 0.33 are denoted by boldfaced values. Note that these stress tensors could generate failure in the intact rock depending on its internal cohesion, since the average internal friction angle of rocks was found to be 30° [*Twiss and Moores*, 1992].

assumed to be laterally homogeneous within the study area; (2) σ_H direction is between N145° and N160°; (3) the R-value of the stress tensor is between 0.25 and 0.45; and (4) the maximum principal stress is either vertical (normal faulting regime) or horizontal (strike-slip faulting regime).

[41] As input we applied depth dependent stress fields described by equation (3). The orientation and magnitude of the input stress tensors were in agreement with the observed end-members of the σ_H direction and the R-value range. Thus, slip tendency and slip direction were calculated for stress tensors having 0.25 and 0.45 R-value as well as N145° and N160° σ_H direction. Every possible R-value-σ_H orientation combination was modelled both in normal faulting and in strike-slip faulting stress regimes. Since stress tensors with different principal stress ratios can have the same R-value, we modelled the σ_h/σ_H ratio between 0.2 and 0.9 with 0.1 steps for both R-value end-members. Although there are published data sets available constraining the σ_h/σ_H ratio ($\sigma_h/\sigma_H \geq 0.6$ [*Grünthal and Stromeyer* 1994]) we wanted to study the resolved stresses caused by stress fields having also lower σ_h/σ_H ratios. This altogether resulted in 64 different input stress tensors (Table 1).

[42] To constrain the likelihood of possible fault reactivation in the different input stress fields, mechanical parameters for the faults as well as pore pressure values should be considered. Despite the rapid late Cenozoic sediment loading, pore fluid overpressure is not observed in the area, therefore it is neglected. There are no direct or indirect measured data available regarding the cohesion and frictional coefficients of the faults in the area. In this regard therefore, we have to rely upon published data sets. Following other authors [e.g., *Brace and Kohlstedt*, 1980; *Reches*, 1987; *Twiss and Moores*, 1992; *Zoback*, 1992; *Plenefisch and Bonjer*, 1997] we consider the faults to be cohesionless. As it was discussed earlier, frictional coefficients ranging from 0.3–0.6 were determined for large faults in normal pore pressure conditions. For every modelled fault we adopted this range of frictional coefficients as the threshold of possible slip.

3.2. Modeling Results

[43] Due to the large number of input stress tensors, not all of the results are presented in the form of a 3-D perspective view. Instead, for every fault the minimum and maximum of the average slip tendency and slip direction values were calculated. The minimum and maximum values correspond to the two end-members of the modelled R-value range (0.25 and 0.45). The range of average slip tendencies is displayed as the function of the σ_h/σ_H ratio (Figure 5). For a given R-value the average shear direction does not change with the σ_h/σ_H ratio, therefore for the shear directions no such graph was created. It should be noted that on Figures 6 and 7, where the 3-D pattern of slip tendencies and slip directions are shown, only a ~1500 m high strip in the center of the faults is visualised. We did this in order to prevent the view of the faults from being obstructed by other faults. In reality the depth range of the faults are much larger.

[44] For the sake of clarity the faults were clustered into five groups based on the characteristics of the ST-σ_h/σ_H curves (Figure 5). In the case of group 1–3, the faults belonging to the same group have similar orientations. Group 1 is the most packed group (25 faults) containing faults having ~N145–150° orientation (see Figure 4b). Group 2 and 3 contain faults with ~N130–140° and ~N120° orientations respectively. Group 4 contains faults mainly from the southernmost Limburg area having less consistent orientations and therefore less consistent ST-σ_h/σ_H curve shape than faults in the previous groups. Group 5 is the "group of outliers" (6 faults also mainly from Limburg) which contain faults with ST-σ_h/σ_H curve characteristics not fitting into any of the previous groups. This group is not represented on Figure 5.

[45] The average values (Figure 5) and the 3-D patterns (Figure 6) indicate that the slip tendency is a decreasing function of the σ_h/σ_H ratio both for normal faulting and for strike-slip faulting stress regimes. It is also clear that the slip tendency of the modelled faults is always lower for strike-slip faulting stress tensors than for normal faulting ones, indicating that reactivation would be more difficult if the σ_2 were vertical. Neither of the faults are likely to reactivate if the σ_h/σ_H ratio is larger than 0.65 for normal faulting and 0.5 for strike-slip faulting regimes, since then the calculated slip tendency is lower than 0.3.

[46] In all the modelled stress tensor cases, there is an observable difference in slip tendency between faults belonging to group 1, 2 and 3. When the stress tensor describes normal a faulting regime, group 1 and 3 has respectively the highest and the lowest average slip tendency indicating, that faults in group 1 are more suitably oriented to these stress tensors than faults in group 3. This is expected considering the orientations of the faults within these groups. The σ_h/σ_H ratio where the slip tendency overcomes the upper limit of the reasonable frictional coefficient (0.6) is different for every group. For normal

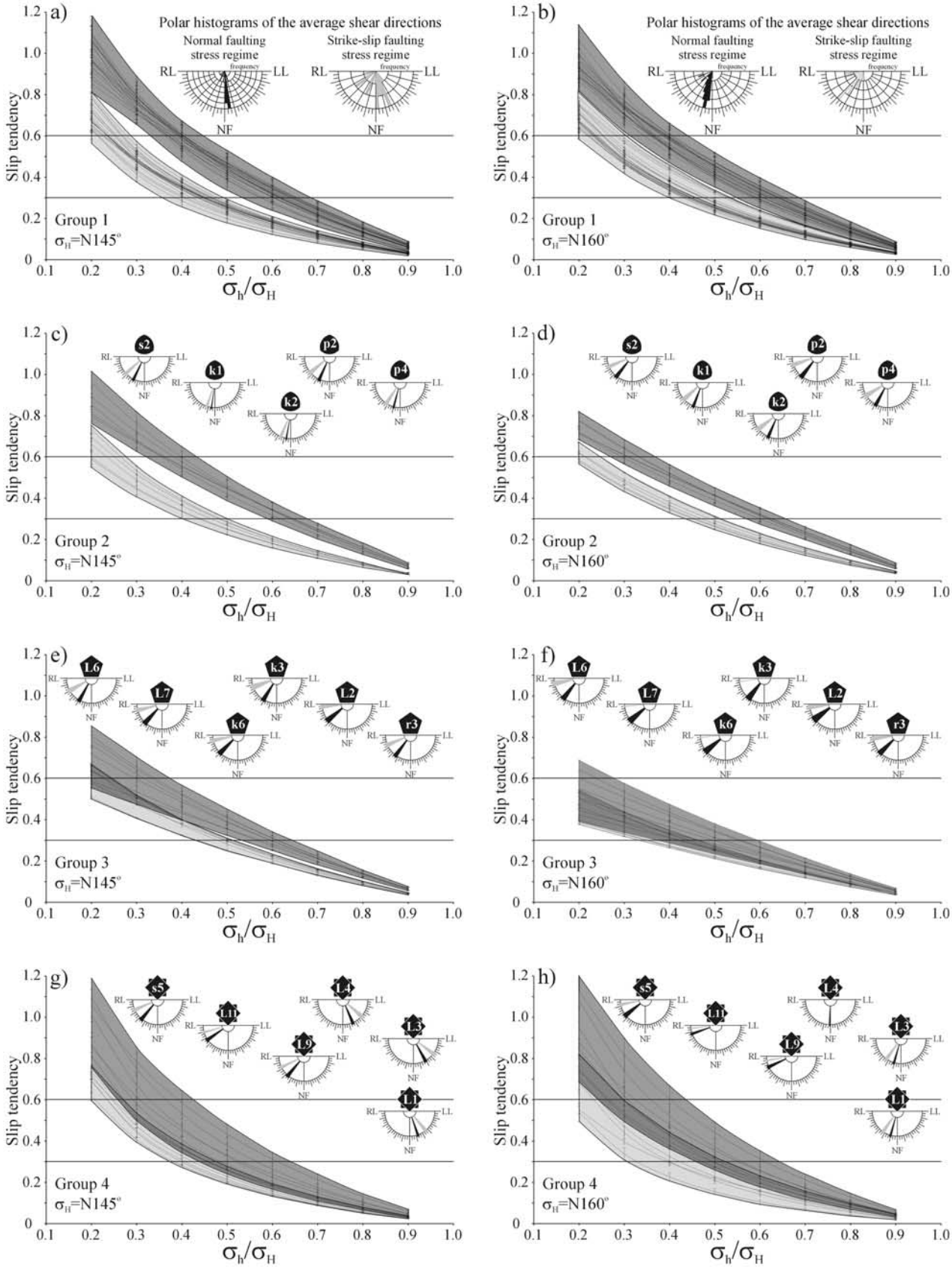
a)
Polar histograms of the average shear directions
Normal faulting stress regime
Strike-slip faulting stress regime
RL
LL
NF
frequency
Slip tendency
Group 1
σH=N145°
σh/σH
b)
Group 1
σH=N160°
c)
s2
k1
p2
p4
k2
Group 2
σH=N145°
d)
Group 2
σH=N160°
e)
L6
L7
k3
L2
k6
r3
Group 3
σH=N145°
f)
Group 3
σH=N160°
g)
s5
L11
L4
L3
L9
L1
Group 4
σH=N145°
h)
Group 4
σH=N160°

Figure 5.

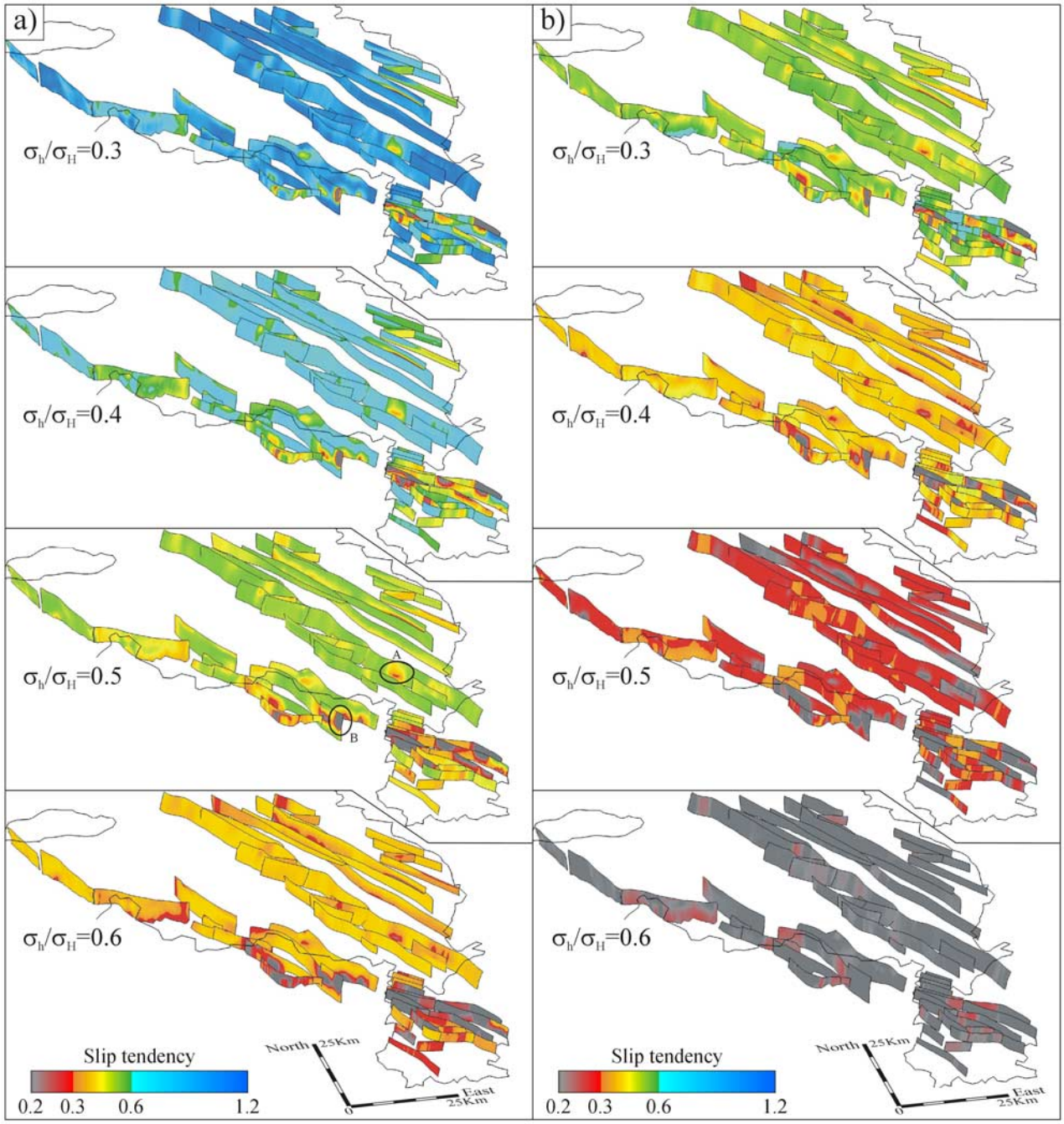

Figure 6. Perspective view of the 3-D faults with slip tendency patterns calculated for input stress tensors having different σ_h/σ_H ratios and σ_H directions of N145 degrees. Vertical scale is 4× exaggerated. (a) Stress tensors describing a normal faulting regime. (b) Strike-slip-faulting stress tensors. The R-value of the stress tensor was modelled as 0.45 for Figure 6a and as 0.25 for Figure 6b representing the maximum slip tendencies within the modelled R-value range.

Figure 5. Average calculated slip tendency of the faults as the function of the σ_h/σ_H ratio. The shaded areas indicate the total range of possible slip tendencies within the given group of faults. Light shading is for strike-slip-faulting stress tensors, and dark shading is for stress tensors describing a normal faulting stress regime. Insets for Figures 5a and 5b show the polar histograms of the average shear directions for group 1. Other insets (Figures 5c–5h) show the average shear direction range for the given fault representing the two end-members of the R-value range (0.25–0.45). Black is to indicate normal-faulting stress tensors, and light shading is for strike slip faulting stress tensors. The left and right panels of Figure 5 correspond to stress tensors with σ_H orientation being N145° and N160°.

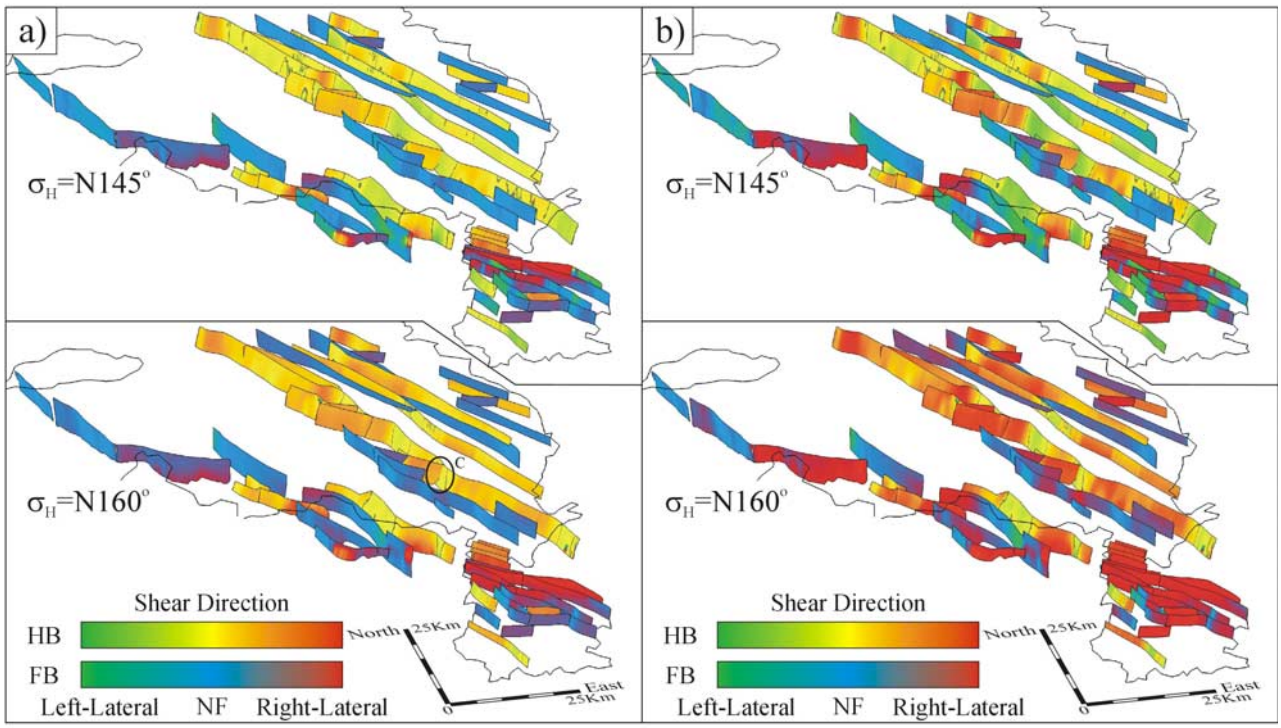

Figure 7. Perspective view of the 3-D faults with shear direction patterns calculated for input stress tensors having different σ_H directions of N145 and N160 degrees. Vertical scale is 4× exaggerated. (a) Stress tensors describing normal faulting regime. (b) Strike-slip-faulting stress tensors. The R-value of the stress tensor was modelled as on Figure 6. HB, hangingwall-block; FB, footwall-block; NF, normal faulting (dip slip shear direction).

faulting stress regimes it is between 0.4 (group 1) and 0.3 (group 3), for strike slip faulting regimes it is lower than ~0.25. This means in other words, that either a reduced slip threshold or stress tensors with very low σ_h/σ_H ratio is needed to reliably say that the faults are active in the study area. To provide more accurate predictions, better constraints regarding the stress magnitudes and the frictional parameters of the faults would be required.

[47] The slip tendency difference observed for stress tensors having identical magnitudes but different orientations can be characterized by a constant shift, therefore the 3-D slip tendency patterns are only provided for the N145° case (Figure 6). In cases where the stress field describes normal faulting regime, all of the faults experience a slip tendency drop if the stress field is rotated to N160° (Figure 5). This drop is the largest for group 3 (~1–1.5). An opposite effect (slightly higher ST values) can be observed in examples where the stress field is within the strike-slip-faulting regime.

[48] Due to the relatively low R-value of the input stress tensors, there is a moderate to significant strike-slip component in the shear vectors even if the stress tensor describes normal faulting regime and the angle between the fault strike and the orientation of σ_H is small (see Figure 5 and the greenish and reddish cast on Figure 7a). Shear directions with minor (0–15°) lateral components was found only along the Peel Boundary Fault (p1 fault) and along other faults in group 1. This is expected since σ_H of the modelled stress tensors is quasi parallel to these faults. Since the Peel Boundary Fault consists of differently oriented segments, along this fault there is a slight alternating left- and right-lateral shear component (greenish and reddish cast respectively) superimposed onto the pure dip-slip (yellow) component (Figure 7).

[49] If the stress tensor describes a strike-slip-faulting regime, the lateral component of the shear direction is more important even if the σ_H is oriented as N145. If σ_H has N160 direction even the faults in group 1 are predicted to have oblique shear directions, while other faults, especially in the southernmost Limburg area (L-faults) show pure right-lateral shear directions (red colors on Figure 7).

[50] From the results presented above we conclude that the maximum principal stress of the stress field in the area is more likely vertical (normal faulting regime) than horizontal. This conclusion is built upon the following: (1) if the stress tensor describes a strike-slip faulting regime then a much lower σ_h/σ_H ratio is required to overcome a given slip threshold; (2) very low σ_h/σ_H ratios would be in disagreement with σ_h/σ_H predictions based on finite element modeling [*Grünthal and Stromeyer*, 1994]; (3) in case of a stress tensor having a vertical σ_2, a very low slip threshold (0.1–0.2) would be required to reactivate the faults within a reasonable range of σ_h/σ_H ratios, which would suggest very low frictional coefficients or high pore fluid pressures, which are not observed in the area.

4. Discussion

4.1. Reliability of the Results

[51] In this paper slip tendency and slip direction patterns were calculated for 3-D fault models in different tectonic

stress fields. The results were presented as detailed 3-D patterns along the faults as well as average values. The reliability of the results depends on the reliability of the fault models and the validity of the input stress field. The fault models in the area are based on regional mapping data and were created in GOCAD from fault trace lines. Due to inconsistency in these data, some fault models contain unreal features, which are also reflected in the slip tendency and slip direction patterns. Locations A and B on Figure 6 are two typical examples of this, where a small area with a low slip tendency value is surrounded by slip tendencies with twice the value. These are artifacts since it would be incorrect to think that a small patch in the middle of the fault is locked while the surroundings are active. We took also the average of the calculated parameters along the faults, since it sometimes provides a more reliable representation of slip tendencies and slip directions than the detailed 3-D pattern.

[52] This study revealed that all shear directions calculated for some fault models in the Limburg area (L9, L10, L11, L12, L13, L14) contain significant lateral components even if the input stress tensor describes a normal faulting regime. The analysis of river terraces displaced by the Feldbiss Fault Zone (L9, L10, L11, L12) however revealed dip slip reactivation of these faults in the Quaternary [*Houtgast et al.*, 2002]. The observed difference could be explained by the fact, that the 3-D models of the mentioned faults are very steep (L12 is almost vertical). We suggest that these geometrical fault models (and the results) are not reliable and should be reviewed.

[53] The validity of the input stress field (and therefore the reliability of the results) depends on the general style of deformation within the study area. In cases, where the stress tensor described a strike-slip-faulting regime, the lateral component of the calculated shear directions was found to be significant. As discussed earlier, in a scenario like this the curvature of the fault bends and the spacing between faults are very important parameters, which could deviate the local stress pattern from the stress pattern calculated using the Wallace-Bott hypothesis. Since we used the regional stress field as input, and since our approach does not take into account distorting factors such as fault interaction a higher uncertainty should be considered in cases of strike slip faulting stress regimes. Precise evaluation of the amount of uncertainty, however, was not performed, since a more sophisticated method would be required to do that.

[54] Kinematic interaction between intersecting faults could be significant in some cases in the study area even if the stress field describes normal faulting. Location C on Figure 7 is an example, where besides the dominant dip-slip component a slight left- and right-lateral component is present in the shear direction along two intersecting faults. Along this and similar intersection lines there is a discrepancy in the shear directions between the two faults, the calculated slip tendency therefore is also expected to be less reliable.

4.2. Comparison of the Results With Observations and Other Studies

[55] On Figure 8 the depth of the base Quaternary horizon as well as its gradient map is shown. We use this map as well as some published earthquake focal mechanism data to compare the modeling results with observations. As a more likely case we consider only the results where the stress fields described normal faulting regimes.

4.2.1. Quaternary Fault Activity

[56] The calculated slip tendencies are compared with the gradient map of the base Quaternary horizon as a recorder of the Quaternary fault activity. The first important observation is that the largest offsets are found along the Peel Boundary Fault (p1) and the Feldbiss Fault Zone (L11, L9, s6, r3, r2, and r1 faults). These faults were reported to be the neotectonically most active faults in the area [e.g., *Houtgast et al.*, 2002; *Michon and van Balen*, 2004]. As it was discussed earlier, this implies that these faults are primary faults and are interconnected with deeper fractures rather than the slip tendency along them is higher than along other faults in the area. This further suggests, that the small secondary faults related to these boundary faults (almost all of the p faults for example) can not be considered as being independent from the boundary faults: their reactivation is strongly affected by the behavior of the main fault [e.g., *Pace et al.*, 2002; *Martinez-Diaz*, 2002]. Location A on Figure 8 shows a good example of this, where the amount of vertical displacement along the Peel Boundary Fault drops by a factor of two. The "missing" displacement is taken up by the fault p4, which branches from the PBF. As the figure shows however, this interaction decays rapidly away from the intersection point. Therefore, although the main assumptions of our method include independent faults, we propose that the slip tendency and slip direction patterns along faults should always be evaluated in a regional tectonic context.

[57] The second interesting observation is that the majority of the faults which have expression in the Quaternary record are directed as $\sim$N145°, that is parallel to the orientation of the stress field. In other words, the calculated slip tendency being highest for these faults (group 1) in normal faulting stress regimes is in agreement with their Quaternary activity. Faults k3 and k6 (see Figure 4) which are differently oriented than the faults in group 1 always experienced lower slip tendency values during the analysis and do not show activity in the Quaternary. Unfortunately there is no direct correlation between slip tendency and the activity of a given fault. Fault r3 namely is one of the most active faults in the area despite the fact that it is similarly oriented and had similar slip tendency values than faults k3 and k6. This again emphasises that the tectonic context of a fault and its position in the fault hierarchy is equally if not more important regarding fault reactivation than fault orientation: k3 and k6 are short secondary faults, while r3 forms part of the southern boundary fault zone (FFZ). Displacement along this segment which was predicted to have $\sim$30° of lateral component is suggested to be dependent on the displacement along adjacent segments (s6 and r2) which are optimally oriented to the stress field.

4.2.2. Earthquake Focal Mechanisms

[58] *Camelbeeck et al.* [1994] suggested that a simple plane extrapolation of faults known from the uppermost crust to the lower crust is unsatisfactory in the case of the Roer Valley Rift System. We used 10 published earthquake focal mechanisms presented on Figure 8 to compare displacements in the deeper part of the seismogenic layer with calculated shear directions believed to be valid in the upper

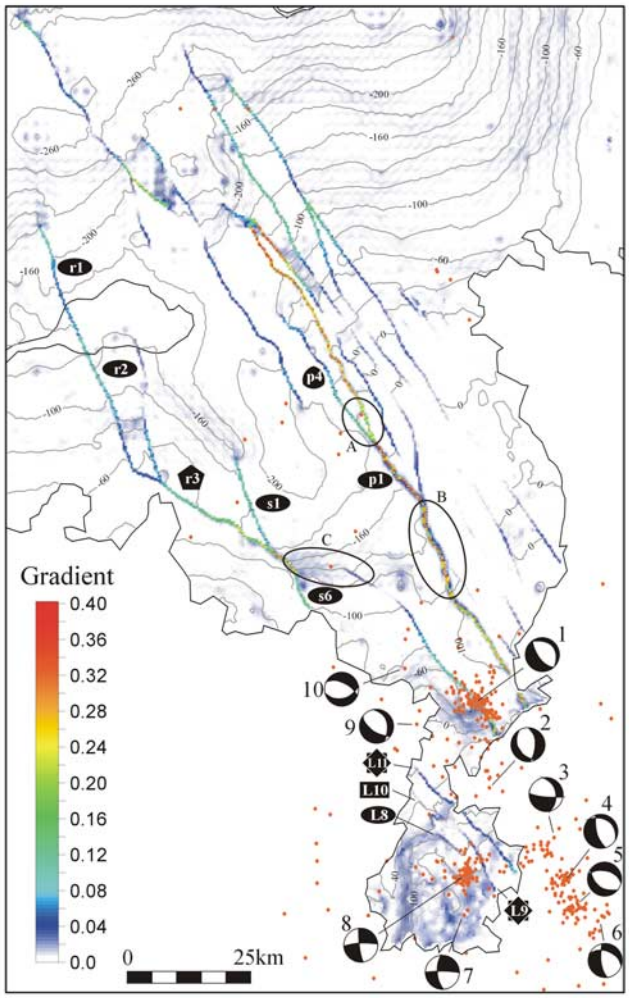

Figure 8. Depth map of the base Quaternary horizon (contours) and its gradient map (data from *de Mulder et al.* [2003]). Higher gradients imply larger offsets. Earthquakes of the last century are shown in red. Focal mechanisms are from *Camelbeeck and van Eck* [1994]. One should bear in mind that the southernmost area is characterized by a hilly topography. See text for discussion.

few kilometres of the crust. With the exception of events 7 and 8 these earthquakes occurred along the SW dipping PBFZ and the NE dipping FFZ and therefore their epicentres are located in the middle of the graben. The nodal planes of events 1, 4, 6 and 9 correlate well with the general strike of the Peel Boundary and Feldbiss faults. Other events (events 2, 3, 5 and 10) are suggested either to occur along differently oriented segments (similar to segment marked by B on Figure 8) or along branching faults of the main boundary faults. Faults with directions parallel to the nodal planes of events 3, 5, and 10 are present in the basement and the Quaternary geological record reflects displacement along them (fault r3 and its continuation (Location C on Figure 8)). The joint presence of earthquakes along the PBF/FFZ and along branching faults suggests that the influence of the boundary faults onto closely related secondary faults is important in the area.

[59] The focal mechanisms of events 7 and 8 suggest pure lateral displacement along very steep planes. The orientations found for the nodal planes (∼E-W or N-S) are also present in the subsurface fault pattern: L2, L6, and L7 for example. However, there is some discrepancy between the predicted slip direction for these faults and the focal mechanism of events 7 and 8 (oblique slip vs. pure strike-slip), which could be attributed to the different dipping angle. This on one hand could suggest that fault dip is different in the deeper than in the uppermost part of the crust in this area. On the other hand it could also be attributed to the fact, that due to the morphology and the lack of high quality seismic surveys the fault models in this southernmost area are less reliable.

[60] The focal mechanisms of events 1–6 and 9–10 describe dip-slip movements with no or minor strike-slip component, which is in agreement with the modeling results. This on one hand is not surprising since the input stress tensors used in our analysis were constrained by the results of stress inversion methods, which are based on the same principles as our forward method. On the other hand it is interesting to see that the slip directions observed in the deeper part of the seismogenic layer correlate reasonably well with the calculated shear directions using fault data from the uppermost crust. This suggests that as a first order approximation both the principal stress ratios and the fault orientations can be considered invariable throughout the whole seismogenic layer in the Roer Valley Rift System. Quasi depth independent principal stress ratios were found to be reasonable in intraplate conditions [*Jaeger and Cook*, 1976; *Brudy et al.*, 1997; *Plenefisch and Bonjer*, 1997; *Ito and Zoback*, 2000].

4.2.3. Comparison With Other Studies

[61] Based on the finite element approach *Grünthal and Stromeyer* [1994] modelled the present-day state of stress in Central and Western Europe induced by far field processes such as the push of Africa and the opening of the Atlantic. They determined that the ratio of the minimum and maximum horizontal principal stresses are nowhere lower than 0.6. Our results revealed that the calculated slip tendencies at $\sigma_h/\sigma_H \geq 0.6$ are below or just above 0.3. Below the slip tendency of 0.3 the faults are likely to be locked, which is in disagreement with the Quaternary record. The disagreement on one hand could be resolved by assuming that the slip threshold of the faults is lower (0.2–0.3) than it was assumed. On the other hand *Grünthal and Stromeyer* [1994] used regional data to determine the $\sigma_h/\sigma_H > 0.6$ relation: local effects were not taken into account. For example deep seismic profiles across the Netherlands suggest thicker crust with different rheological built-up in the London-Brabant Massif than in the Roer Valley Graben [*Rijkers and Duin*, 1994]. Other studies [*Illies and Fuchs*, 1983] suggested oppositely rotating crustal blocks in the Rhenish Massif as an explanation for the opening of the Lower Rhine Embayment. This process together with a heterogeneous rheology could generate concentrated excess stresses in the SE Netherlands. This could result in somewhat lower σ_h/σ_H ratio in the crust being more favourable for fault reactivation. However, significant lowering of the σ_h/σ_H ratio by these local effects is not expected. This suggests that in order to explain the observed fault activity slip thresholds

being in the lower section of the adopted range (between slip tendency of 0.3 and 0.4) have to be assumed.

5. Conclusions

[62] 3-D geometrical fault models give an excellent opportunity to study the 3-D pattern of forces acting along faults in a certain tectonic stress field. Using these models in combination with assumptions of the tectonic stresses around the faults, the shear and normal stresses at every location of the faults can be quickly calculated. Although the contact stresses calculated using the method presented in this paper represent only a first order approximation of the real stresses around the faults, the patterns of slip tendency and shear direction provide useful, 3 dimensional constraints about the likelihood and style of fault reactivation.

[63] In the Roer Valley Rift System earthquake focal mechanism studies are inconclusive about whether the stress regime is normal- or strike-slip faulting. Analysis of the slip tendency and shear direction patterns in the Roer Valley Rift System demonstrates that the faults are more likely to reactivate in a normal faulting stress regime. In a strike-slip faulting regime a very low σ_h/σ_H ratio would be required to reactivate the faults, which is not in accordance with continent-scale modeling studies. Even in case of normal faulting stress regimes high probabilities of fault reactivation (ST > 0.6) were only obtained at σ_h/σ_H ratios lower than $\sim$0.4, which is still lower than that determined by these European-scale studies ($\sim$0.6). In order to explain the observed fault activity within a reasonable range of tectonic stress magnitudes a slip threshold (frictional coefficient) of 0.3–0.4 and stress tensors with a 0.5–0.6 σ_h/σ_H ratio would be required. Slight discrepancies between the σ_h/σ_H ratios suggested by our method and those inferred from continent-scale modeling could be attributed to local effects.

[64] In case of normal faulting stress regimes the case study demonstrated that the faults which were active in the Quaternary have the highest slip tendency values. In addition there is a reasonably good correlation between the calculated and observed slip directions represented by earthquake focal mechanisms. These results suggest that in the Roer Valley Rift System the fault models mapped in the uppermost part of the crust are suitable to constrain fault behavior even in the deeper parts of the seismogenic layer. On the other hand model results also show, that knowledge of the hierarchy and the regional tectonic context of the faults are required to explain the slip tendency and shear direction patterns. For example, secondary faults in the close vicinity of the Peel Boundary and Feldbiss Faults interconnected with deep crustal fractures should not be considered to be independent.

[65] **Acknowledgments.** We thank Associate Editor Teruo Yamashita, Dr. Richard Lisle and an anonymous reviewer for the thoughtful and constructive remarks. This research was carried out as a co-operation between the Tectonic Department of the Vrije Universiteit of Amsterdam and the Geoenergy Department of the Netherlands Institute of Applied Geosciences TNO Utrecht. We are grateful to T. Cornu, L. Michon for their remarks and to C. Pascal and M. Gerbault for the discussions and for their constructive criticism and helpful advice.

References

Ahorner, L. (1975), Present-day stress field and seismotectonics block movements along major fault zones in Western Europe, *Tectonophysics*, *29*, 233–249.

Alaniz-Alvarez, S. A., G. Tolson, and A. F. Nieto-Samaniego (2000), Assessing fault reactivation with the ReActiva Program, *J. Geosci. Edu.*, *48*, 651–657.

Angelier, J. (1984), Tectonic analysis of fault slip data, *J. Geophys. Res.*, *89*, 5835–5848.

Angelier, J. (1990), Inversion of field data in fault tectonics to obtain the regional stress, part 3. A new rapid direct inversion method by analytical means, *Geophys. J. Int.*, *103*, 363–376.

Angelier, J. (2002), Inversion of earthquake focal mechanisms to obtain the seismotectonic stress, IV, A new method free of choice among nodal planes, *Geophys. J. Int.*, *150*, 588–609.

Bergerat, F. (1987), Stress field in the European platform at the time of Africa-Eurasia collision, *Tectonics*, *6*, 99–132.

Bott, M. H. P. (1959), The mechanics of oblique slip faulting, *Geol. Mag.*, *96*, 109–117.

Brace, W. F., and D. L. Kohlstedt (1980), Limits on lithospheric stress imposed by laboratory experiments, *J. Geophys. Res.*, *85*, 6248–6252.

Brudy, M., M. D. Zoback, K. Fuchs, F. Rummel, and J. Baumgärtner (1997), Estimation of the complete stress tensor to 8 km depth in the KTB scientific drill holes: Implications for crustal strength, *J. Geophys. Res.*, *102*, 18,453–18,475.

Byerlee, J. D. (1978), Friction of rocks, *Pure Appl. Geophys.*, *116*, 615–626.

Camelbeeck, T., and T. van Eck (1994), The Roer Valley Graben earthquake of 13 April 1992 and its seismotectonic setting, *Terra Nova*, *6*, 291–300.

Camelbeeck, T., T. van Eck, R. Pelzing, L. Ahorner, J. Loohuis, H. W. Haak, P. Hoang-Trong, and D. Hollnack (1994), The 1992 Roermond earthquake, the Netherlands, and its aftershocks, *Geol. Mijnbouw*, *73*, 181–197.

Cashman, P. H., and M. A. Ellis (1994), Fault interaction may generate multiple slip vectors on a single fault surface, *Geology*, *22*, 1123–1126.

de Mulder, E. F. J., M. C. Geluk, I. Ritsema, W. E. Westerhoff, and Th. E. Wong (2003), De ondergrond van Nederland, 379 pp., Neder. Org. voor toegepast-natuurwet. onderzoek TNO, Utrecht, Netherlands.

Dirkzwager, J. B. (2002), Tectonic modelling of vertical motion and its near surface expression in the Netherlands, Ph.D. thesis, 156 pp., Netherlands Res. Sch. of Sediment. Geol., *Publ. 20020901*, Vrije Univ., Amsterdam, Netherlands.

Dirkzwager, J. B., J. D. van Wees, S. A. P. L. Cloetingh, M. C. Geluk, B. Dost, and F. Beekman (2000), Geo-mechanical and rheological modelling of upper crustal faults and their near-surface expression in the Netherlands, *Global Planet. Change*, *27*, 67–88.

Dupin, J. M., W. Sassi, and J. Angelier (1993), Homogeneous stress hypothesis and actual fault slip: A distinct element analysis, *J. Struct. Geol.*, *15*, 1033–1043.

Ferrill, D. A., and A. P. Morris (2003), Dilational normal faults, *J. Struct. Geol.*, *25*, 183–196.

Geluk, M. C., E. J. Th. Duin, M. Dusar, R. H. B. Rijkers, M. W. van den Berg, and P. van Rooijen (1994), Stratigraphy and tectonics of the Roer Valley Graben, *Geol. Mijnbouw*, *73*, 129–141.

Gephart, J. W. (1990), Stress and the direction of slip on fault planes, *Tectonics*, *9*, 845–858.

Gephart, J. W., and D. W. Forsyth (1984), An improved method for determining the regional stress tensor using earthquake focal mechanism data: Application to the San Fernando earthquake sequence, *J. Geophys. Res.*, *89*, 9305–9320.

Grauls, D. J., and J. M. Baleix (1994), Role of overpressures and in situ stresses in fault-controlled hydrocarbon migration: A case study, *Mar. Pet. Geol.*, *11*, 734–742.

Grünthal, G., and D. Stromeyer (1994), The recent crustal stress field in Central Europe sensu lato and its quantitative modeling, *Geol. Mijnbouw*, *73*, 173–180.

Hardebeck, J. L., and E. Hauksson (2001), Crustal stress field in southern California and its implications for fault mechanics, *J. Geophys. Res.*, *106*, 21,859–21,882.

Hobbs, B. E., A. Ord, and C. Marone (1990), Dynamic behavior of rock joints, in *Rock Joints*, edited by N. Barton and O. Stephansson, pp. 435–445, A. A. Balkema.Rotterdam, Netherlands.

Houtgast, R. F., and R. T. van Balen (2000), Neotectonics of the Roer Valley rift system, the Netherlands, *Global Planet. Change*, *27*, 131–146.

Houtgast, R. F., R. T. van Balen, L. M. Bouwer, G. B. M. Brand, and J. M. Brijker (2002), Late Quaternary activity of the Feldbiss Fault Zone, Roer Valley Rift System, the Netherlands, based on displaced fluvial terrace fragments, *Tectonophysics*, *352*, 295–315.

Houtgast, R. F., R. T. van Balen, C. Kasse, and J. Vandenberghe (2004), Late Quaternary tectonic evolution and postseismic near surface displacements along the Geleen Fault (Feldbiss Fault Zone-Roer Valley Rift System, the Netherlands), based on trenching, Netherlands, *J. Geosci.*, in press.

Illies, J. H., and K. Fuchs (1983), Plateau uplift of the Rhenish Massif-introductory remarks, in *Plateau Uplift, The Rhenish Massif: A Case History*, edited by K. K. Fuchs et al., pp. 1–8, Springer-Verlag, New York.

Ito, T., and M. D. Zoback (2000), Fracture permeability and in situ stress to 7 km depth in the KTB Scientific Drillhole, *Geophys. Res. Lett.*, *27*, 1045–1048.

Jaeger, J. C., and N. G. W. Cook (1976), *Fundamentals of Rock Mechanics*, Chapman and Hall, New York.

Klein, R., and M. Barr (1987), Regional state of stress in western Europe, in *Proceedings of the International Symposium on Rock Stress and Rock Stress Measurements*, edited by O. Stephansson, pp. 33–45, Centek, Lulea, Sweden.

Kooi, H., M. Hettema, and S. Cloetingh (1991), Lithospheric dynamics and the rapid pliocene-quaternary subsidence phase in the southern north sea basin, *Tectonophysics*, *192*, 245–259.

Kooi, H., P. Johnston, K. Lambeck, C. Smither, and R. Molendijk (1998), Geological causes of recent (~100 yr) vertical land movements in the Netherlands, *Tectonophysics*, *299*, 297–316.

Krantz, R. W. (1991), Measurements of friction coefficients and cohesion for faulting and fault reactivation in laboratory models using sand and sand mixtures, *Tectonophysics*, *188*, 203–207.

Malservisi, R., C. Gans, and K. P. Furlong (2003), Numerical modeling of strike-slip creeping faults and implications for the Hayward fault, California, *Tectonophysics*, *361*, 121–137.

Martinez-Diaz, J. J. (2002), Stress field variation related to fault interaction in a reverse oblique-slip fault: The Alhama de Murcia fault, Betic Cordillera, Spain, *Tectonophysics*, *356*, 291–305.

Michon, L., and R. T. van Balen (2004), Characterisation and quantification of active faulting in the Roer Valley Rift System based on high precision Digital Elevation Models, *Quat. Sci. Rev.*, in press.

Michon, L., R. T. van Balen, O. Merle, and H. Pagnier (2003), The Cenozoic evolution of the Roer Valley Rift System integrated at a European scale, *Tectonophysics*, *367*, 101–126.

Morris, A., D. A. Ferrill, and D. B. Henderson (1996), Slip-tendency analysis and fault reactivation, *Geology*, *24*, 275–278.

Müller, G., M. L. Zoback, K. Fuchs, L. Mastin, S. Gregersen, N. Pavoni, O. Stephansson, and C. Ljunggren (1992), Regional patterns of tectonic stress in Europe, *J. Geophys. Res.*, *97*, 1783–1803.

Nieto-Samaniego, A. F., and S. A. Alaniz-Alvarez (1997), Origin and tectonic interpretation of multiple fault patterns, *Tectonophysics*, *270*, 197–206.

Pace, B., P. Boncio, and G. Levecchia (2002), The 1984 Abruzzo earthquake (Italy): An example of seismogenic process controlled by interaction between differently oriented synkinematic faults, *Tectonophysics*, *350*, 237–254.

Pascal, C. (1998), Etude mécanique et modélisation de la fracturation en extension, application au domaine de la Mer du Nord, Ph.D. thesis, 410 pp., Sci. de la Terre, Univ. P. and M. Curie, Paris.

Pascal, C., and J. Angelier (2004), Sortan, an analytical method to determine fault slip as induced by stresses, *Math. Geol.*, in press.

Pascal, C., J. Angelier, R. T. Seland, and C. Lepvrier (2002), A simplified model of stress-slip relationships: Application to the Frøy field, northern North Sea, *Tectonophysics*, *357*, 103–118.

Plenefisch, T., and K. P. Bonjer (1997), The stress field in the Rhine Graben area inferred from earthquake focal mechanisms and estimation of frictional parameters, *Tectonophysics*, *275*, 71–97.

Pollard, D. D., S. D. Saltzer, and A. M. Rubin (1993), Stress inversion methods: Are they based on faulty assumptions?, *J. Struct. Geol.*, *15*, 1045–1054.

Ranalli, G. (1987), *Rheology of the Earth: Deformation and Flow Processes in Geophysics and Geodynamics*, Allen and Unwin, Concord, Mass.

Rebaï, S., H. Philip, and A. Taboada (1992), Modern tectonic stress field in the Mediterranean region; evidence for variation in stress directions at different scales, *Geophys. J. Int.*, *110*, 106–140.

Reches, Z. (1987), Determination of the tectonic stress tensor from slip along faults that obey the Coulomb yield criterion, *Tectonics*, *6*, 849–861.

Rijkers, R. H. B., and E. J. Th. Duin (1994), Crustal observations beneath the southern North Sea and their tectonic and geological implications, *Tectonophysics*, *240*, 215–224.

Rondeel, H. E., and J. S. L. Everaars (1993), Spanning in noordoost Nederland, een breakoutanalyse, in *Eindrapport Multidisciplinair Onderzoek naar de Relatie Tussen Gaswinning en Aardbevingen in Noord-Nederland*, Het Koninklijk Neder, Meteorol. Inst., De Bilt, Netherlands.

Rummel, F. (1986), Stresses and tectonics of the upper continental crust-a review, in *Rock Stress and Rock Stress Measurements* [*International Symposium on Rock Stress and Rock Stress Measurements* [*Stockholm, September 1–3*], *Proceedings*], edited by O. Stephansson, pp. 177–184, Centek Publ., Stockholm, Denmark.

Sibson, R. H. (1985), A note on fault reactivation, *J. Struct. Geol.*, *7*, 751–754.

Sibson, R. H. (1994), Crustal stress, faulting and fluid flow, *Geol. Soc. Spec. Publ.*, *78*, 69–84.

Tenthorey, E., S. F. Cox, and H. F. Todd (2003), Evolution of strength recovery and permeability during fluid-rock reaction in experimental fault zones, *Earth Planet. Sci. Lett.*, *206*, 161–172.

Twiss, R. J., and E. M. Moores (1992), *Structural Geology*, W. H. Freeman, New York.

van den Berg, M. W. (1994), Neotectonics of the Roer Valley rift system. Style and rate of crustal deformation inferred from syn-tectonic sedimentation, *Geol. Mijnbouw*, *73*, 143–156.

van den Berg, M. W., W. Groenewoud, G. K. Lorenz, P. J. Lubbers, D. J. Brus, and S. B. Kroonenberg (1994), Patterns and velocities of recent crustal movements in the Dutch part of the Roer Valley rift system, *Geol. Mijnbouw*, *73*, 157–168.

Wallace, R. E. (1951), Geometry of shearing stress and relation to faulting, *J. Geol.*, *59*, 118–130.

Yamaji, A. (2000), The multiple inverse method: A new technique to separate stresses from heterogeneous fault-slip data, *J. Struct. Geol.*, *22*, 441–452.

Yin, Z. M., and G. Ranalli (1992), Critical stress difference, fault orientation and slip direction in anisotropic rocks under non-Andersonian stress systems, *J. Struct. Geol.*, *14*, 237–244.

Yin, Z. M., and G. Ranalli (1995), Estimation of the frictional strength of faults from inversion of fault-slip data; a new method, *J. Struct. Geol.*, *17*, 1327–1335.

Ziegler, P. A. (1990), *Geological Atlas of Western and Central Europe*, 2nd and completely revised ed., Shell Int. Petr. Mij, The Hague, Netherlands.

Ziegler, P. A. (1994), Cenozoic rift system of western and central Europe: An overview, *Geol. Mijnbouw*, *73*, 99–127.

Zijerveld, L., R. Stephenson, S. Cloetingh, E. Duin, and M. W. van den Berg (1992), Subsidence analysis and modelling of the Roer Valley Graben (SE Netherlands), *Tectonophysics*, *208*, 159–171.

Zoback, M. L. (1992), Stress field constraints on intraplate seismicity in eastern North America, *J. Geophys. Res.*, *97*, 1761–1782.

Zoback, M. L., and M. D. Zoback (1980), Faulting patterns in north-central Nevada and strength of the crust, *J. Geophys. Res.*, *85*, 275–284.

Zoback, M. L., R. E. Anderson, and G. A. Thompson (1981), Cainozoic evolution of the state of stress and style of tectonism of the Basin and Range Province of the western United States, *Philos. Trans. R. Soc. London*, *Ser. A*, *300*, 1454.

G. Bada, S. Cloetingh, and G. Worum, Department of Tectonics, Vrije Universiteit, De Boelelaan 1085, 1081HV Amsterdam, Netherlands. (worg@geo.vu.nl)

H. Pagnier and J.-D. van Wees, Department of Geoenergy, Nederlands Instituut voor Toegepaste Geowetenschappen TNO, Princetonlaan 6, 3508 TA Utrecht, Netherlands.

R. T. van Balen, Department of Quaternary Geology and Geomorphology, Vrije Universiteit, De Boelelaan 1085, 1081HV Amsterdam, Netherlands.